

Photoinduced reactions of chloroacetone in solid Ar: Identification of $\text{CH}_2=\text{COCICH}_3$

Nobuaki Tanaka*, Yoshitaka Urashima, Hiromasa Nishikiori

Department of Environmental Science and Technology, Faculty of Engineering, Shinshu University, 4-17-1 Wakasato, Nagano 380-8553, Japan

* Corresponding author. Fax: +81 26 269 5550.

E-mail address: ntanaka@shinshu-u.ac.jp (N. Tanaka).

ABSTRACT

The UV light-induced reactions of chloroacetone in a cryogenic Ar matrix were investigated using infrared spectroscopy. The photoinduced isomerisations of *gauche*-chloroacetone to *syn*-chloroacetone and hypochlorous acid 1-methylethenyl ester were confirmed by comparing the experimental and calculated spectra. In addition, the photolysis products were found to be $\text{CH}_2=\text{C}=\text{O}$ and a cyclopropanone...HCl complex. The cyclopropanone...HCl complex was further decomposed into $\text{CH}_2=\text{CH}_2$, CO and HCl. The hypochlorous acid 1-methylethenyl ester was further isomerised to 2-chloro-2-methyloxirane.

Keywords: chloroacetone; Ar matrix; rotational isomerisation; photolysis; hypochlorous acid 1-methylethenyl ester ($\text{CH}_2\text{COCICH}_3$)

1. Introduction

In the past four decades, halogenated volatile organic compounds (VOCs) have captured the attention of environmental chemists and photochemists because of their role in the depletion of the ozone layer [1]. The VOCs react in the atmosphere leading to the formation of secondary organic aerosols [2], which affect the Earth's radiative balance [3].

The reactions of chloroacetone with OH and Cl have been investigated from an experimental [4] and a theoretical [5] point of view. Hydrogen atom abstraction from a $-\text{CH}_2\text{Cl}$ group was found to be a dominant initial process. Waschewsky et al. found the evidence of competing C–Cl and C–C bond fission reactions during the photolysis of chloroacetone vapor at 308 nm [6]. Kitchen et al. determined the absolute branching ratio between C–Cl and C–C bond fission at 308 nm to be 4.63:1.0 at 180°C [7]. Alligood et al. determined a branching ratio of 11:1 upon excitation at 193 nm [8]. The conformations of chloroacetone have been studied using vibrational spectroscopy [9-11],

electron diffraction [12], NMR spectroscopy [13] and theoretical methods [11-13]. In all of these studies, two conformers have been proven to exist from calculations of the CH₂Cl internal rotation potential: the *gauche* and *syn* conformers have the dihedral angles, $\varphi(\text{Cl}-\text{C}-\text{C}-\text{O})$, of 138(7)–155° and 0.0–5.5°, respectively. The *gauche* conformer was more stable in the vapor state, while the *syn* conformer was predominant in the liquid state. In solution, the *syn/gauche* ratio increased with solvent polarity [10, 13]. However, there is little information available on the photochemistry of chloroacetone trapped in a rare gas matrix.

The present study investigates photoinduced reactions of chloroacetone trapped in solid Ar. Owing to the narrower bandwidth and lower complexity of the spectra obtained in the matrix-isolated species compared with that of spectra of the vapor or liquid state, the absorption bands of the different conformers can be separated. Because of the matrix cage effect, the fragment species formed by photodissociation cause the addition or abstraction reaction to occur within the available energy. As a result, the coexistence of the *gauche* and *syn* conformers in chloroacetone was confirmed. The infrared bands of the less stable conformer were separated and assigned. Moreover, the photolysis products caused by the initial C–Cl bond fission were identified.

2. Experimental

Chloroacetone (Wako Pure Chemicals Industries, Ltd.) was purified by a freeze–pump–thaw cycle at 77 K and was diluted with Ar gas (Nippon Sanso, Japan, 99.999 % purity) to approximately 1/500 (0.4 Torr chloroacetone and 200 Torr Ar). It was then slowly sprayed onto a CsI plate cooled by a closed-cycle helium refrigerator (Iwatani CryoMini M310/CW303) to approximately 7 K. The infrared absorption spectra were measured in the 3500–700 cm⁻¹ range with a resolution of 1.0 cm⁻¹ using a SHIMADZU FTIR 8300 spectrophotometer equipped with a liquid-nitrogen-cooled MCT detector. Each spectrum was obtained by acquiring 128 scans. Under the sample conditions mentioned above, the populations of conformers just after deposition were assumed identical to those at the temperature of the gaseous sample just before deposition (298 K). The photoexcitation effect was examined by irradiating the deposited samples with UV light. A Xe short arc lamp (HAMAMATSU, C2577) with a sharp-cut filter (HOYA UV-29) was used as the UV light source combined with a water filter to avoid thermal radiation.

For product identification and energetic considerations, molecular orbital calculations were performed using the GAUSSIAN 09 program [14]. Geometry optimizations were performed using Becke's three-parameter hybrid density functional

in combination with the Lee–Yang–Parr correlation functional (B3LYP) [15, 16] and MP2 with the aug-cc-pV(T+d)Z or 6-311++G(2d,2p) basis set. Harmonic vibrational frequency calculations were performed in order to confirm the predicted structures as local minima or transition states and to elucidate the zero-point vibrational energy corrections. An anharmonic vibrational frequency calculation was performed at the B3LYP/6-311++G(2d,2p) level. The vertical transition energies of the parent and intermediate species were calculated at the TD B3LYP/aug-cc-pV(T+d)Z level and at the SAC-CI/D95+(d,p)//CCSD/D95+(d,p) level. Vibrational energy distribution analysis was performed using VEDA 4 [17].

3. Results and discussion

3.1 Separation and assignment of the infrared bands of the less stable conformer

A chloroacetone/Ar mixture was deposited on a CsI window (chloroacetone/Ar = 1/500). In the infrared spectrum obtained after deposition, strong bands were observed at 1738 and 1360 cm^{-1} , which were attributed to the C=O stretching and CH_3 symmetric deformation vibrations of chloroacetone, respectively [11]. Figure 1 shows (a) the observed infrared difference spectrum obtained by subtracting the spectrum measured before UV irradiation from the one measured after 70 min of irradiation without the UV-29 filter and (c) the calculated infrared difference spectra of chloroacetone, where the upward and downward bands of the calculated spectra correspond to those of the *syn* and *gauche* conformers, respectively. The UV irradiation resulted in a decrease or an increase in intensities of the bands due to a reactant and the appearance of new bands. The observed and calculated wavenumbers of the product bands are given in Table 1. The bands that increased at 1761 and 1298 cm^{-1} were also present in the as-deposited spectrum. The calculated infrared spectra at the B3LYP/6-311++G(2d,2p) level with anharmonic treatment reproduced well the observed spectrum. Comparison of the observed and calculated spectra indicates that the bands that decreased and increased upon UV irradiation correspond to those of the *gauche* and *syn* conformers, respectively. The increased bands at 1761, 1298, 1158, 838 and 767 cm^{-1} were assigned to C=O stretching, CH_2 wagging, CH_3 rocking, CH_2 rocking and C–Cl stretching vibrations of *syn*- $\text{CH}_2\text{ClCOCH}_3$, respectively. This conformation change was also observed when the irradiation was conducted with the UV-29 filter.

Taking into consideration the solvent dependence of the ^{13}C NMR spectra, Doi et al. determined that the energy difference between the two conformers was 1.7 kcal mol^{-1} in the vapor phase [13]. The calculation at the B3LYP/aug-cc-pV(T+d)Z level

also shows that the *gauche* conformer is more stable than the *syn* conformer by 1.2 kcal mol⁻¹ and the barrier height is 3.5 kcal mol⁻¹ in the ground state. This means that the *syn/gauche* population ratio before UV irradiation is 0.069/1 at 298 K and that the conversion from the *gauche* to *syn* conformer is not expected to occur at 7 K in the absence of UV irradiation. However, UV irradiation led to an increase in the population of the less stable conformer.

3.2 Identification of additional products

The UV irradiation led to the increase of other bands in the difference spectra besides the vibration bands of the *syn*-chloroacetone. The bands that increased in intensity were classified into three groups (A, B and C) according to their different behavior. Figure 2 shows the changes in the absorbance of the bands at 977, 935, 960 and 838 cm⁻¹ for groups A, B and C, and *syn*-chloroacetone, respectively, upon UV irradiation with and without the UV-29 filter. The absorption bands from group A reached a peak after 300 min irradiation time. The bands from group B showed an increase followed by a decrease during the irradiation period, as shown in Figure 2(a). The absorption bands from group C exhibited an induction period. The band due to *syn*-chloroacetone continued to grow.

The wavenumbers of the bands from group A are similar to those of cyclopropanone measured in Ar [18] except for the bands at 2542 and 2146 cm⁻¹. In the 2800–2500 cm⁻¹ region, an absorption band appeared because of the formation of a hydrogen-bond complex of HCl [19, 20]. Two stationary points were previously predicted for the cyclopropanone...HCl complex from the DFT and MP2 calculations, due to the interaction of the hydrogen atom from HCl with an oxygen atom or a C–C bond in cyclopropanone [21]. The former complex was calculated to be more stable and have a larger shift in wavenumber for the HCl stretching vibration compared to the free HCl. Therefore, the observed wavenumbers were compared with those for the >C=O...HCl complex. The calculated wavenumbers were in good agreement with those observed, as listed in Table 1. The bands at 2542, 1831, 1058 and 976 cm⁻¹ were assigned, respectively, to H–Cl stretching, C=O stretching, C–H in-plane bending and C–H in-plane bending vibrations of the cyclopropanone...HCl complex.

In the ~2140 cm⁻¹ region, two bands were observed at 2146 and 2139 cm⁻¹. The former band behaved as a group A band, and the latter as a group C band. Ketene and CO absorption bands are known to emerge in this region [22-24]. In fact, during the photolysis of chloroacetone in the vapor phase, upon 193 nm excitation, CH₂=C=O was produced via the vibrationally excited CH₂COCH₃ radical [8]. Thus, the band at 2146

cm^{-1} was assigned to C=C=O antisymmetric stretching vibration of $\text{CH}_2=\text{C}=\text{O}$.

The three strong bands at 1681, 935 and 820 cm^{-1} from group B were prominent in an early stage of the irradiation, indicating that the bands from group B are due to one of the primary products. The absorption bands due to the conjugated C=O stretching vibration and C=C stretching vibration are known to appear in the ~ 1680 cm^{-1} region. The band at 935 cm^{-1} would indicate the presence of a $>\text{C}=\text{CH}_2$ group. Therefore, we assumed the formation of a recombination product of hypochlorous acid 1-methylethenyl ester, $\text{CH}_2=\text{COCICH}_3$, from the photolysis products of CH_2COCH_3 and Cl. Two conformers, the *syn* and *gauche* forms, were found to exist with the equilibrium dihedral angles of C(H₂)–C–O–Cl calculated to be 0.0 and 127.5°, respectively, at the B3LYP/aug-cc-pV(T+d)Z level, as shown in Figure 3. The *syn* conformer was determined to be more stable by 1.5 kcal mol⁻¹ than the *gauche* conformer. The barrier heights to internal rotation from the *syn* to *gauche* conformer and *gauche* to *gauche* conformer were calculated to be 3.6 and 3.8 kcal mol⁻¹, respectively, at the B3LYP/aug-cc-pV(T+d)Z level. Figure 1(d) compares the calculated spectra of the *syn*- and *gauche*- $\text{CH}_2=\text{COCICH}_3$ conformers. The calculated spectrum of the *syn* conformer was in good agreement with the observed one. Table 2 lists the wavenumber and the assignment of the infrared spectrum for *syn*- $\text{CH}_2=\text{COCICH}_3$. The bands at 1681, 935, 867 and 820 cm^{-1} were assigned to C=C stretching, CH₂ in-plane bending, C–C stretching and CH₂ out-of-plane bending vibrations of *syn*- $\text{CH}_2=\text{COCICH}_3$, respectively. The optimized structural parameters of *syn*- $\text{CH}_2=\text{COCICH}_3$ are listed in Table S1.

The initial growth rate of the bands from group C was smaller than those of the bands from groups A and B, indicating that the bands from group C belong to one of the secondary products. After prolonged irradiation the bands from group C were clearly discernible, as shown in Figure 1(b). The photodissociation of cyclopropanone was studied experimentally [25] and theoretically [26-28]. Thomas and Rodriguez found that $\text{CH}_2=\text{CH}_2$ and CO were the only volatile products resulted upon excitation at a selected wavelength between 292 to 365 nm [25]. The MCSCF calculation showed that photodecarbonylation was initiated predominantly from the lowest excited state, taking the bent-in-plane path, and the ground state $\text{CH}_2=\text{CH}_2$ and CO were produced via the biradical intermediate [26]. Cui et al. found the two conical intersections between the S₁ and S₀ states of cyclopropanone using the state-averaged CASSCF method; one leads to an α -bond fission and the other to two α -bond fissions [27, 28]. In the present experiments, a cyclopropanone \cdots HCl complex was formed. Therefore, during the photolysis, $\text{CH}_2=\text{CH}_2$, CO and HCl would be formed. The characteristic bands belonging to group C were assigned by comparing the observed wavenumbers with

those of the three possible monomers. The band at 2139 cm^{-1} was attributed to CO. The band at 2745 cm^{-1} was assigned to the stretching vibration of H–Cl in $\text{CH}_2=\text{CH}_2\cdots\text{HCl}$. The bands at 1440 and 960 cm^{-1} from group C were assigned, respectively, to the CH_2 scissor and CH_2 wagging vibrations of $\text{CH}_2=\text{CH}_2\cdots\text{HCl}$ [29]. The normalized absorbance changes of the bands at 2745 , 2139 and 960 cm^{-1} also support the concomitant formation of these three species, as shown in Figure S1. As for the photolysis of *syn*- $\text{CH}_2=\text{COCICH}_3$, the vertical transition energies were calculated at the SAC-CI/D95+(d,p) level. The S_1 (3.54 eV), S_2 (4.93 eV) and S_3 (5.16 eV) states were characterized as the $\pi\sigma_{\text{OCl}}^*$ (HOMO \rightarrow LUMO), $n\sigma_{\text{OCl}}^*$ (HOMO–2 \rightarrow LUMO) and $\pi\sigma_{\text{OCl}}^*$ (HOMO–1 \rightarrow LUMO) states with oscillator strengths of 0.0, 0.0039 and 0.0, respectively. Once the *syn*- $\text{CH}_2=\text{COCICH}_3$ is excited upon irradiation, O–Cl bond dissociation occurs to form the CH_2COCH_3 radical and Cl. If the Cl atom recombination occurs at the C2 carbon of CH_2COCH_3 , 2-chloro-2-methyloxirane is formed. The observed and calculated wavenumbers are compared in Table 2. The weak bands at 1381 , 1306 , 1163 and 879 cm^{-1} are tentatively assigned to the vibrations of 2-chloro-2-methyloxirane. No bands attributed to the ethylenic hydrogen atom abstracted products ($\text{H}\ddot{\text{C}}\text{COCH}_3$, methyloxirene and $\text{CH}(=\text{O})\ddot{\text{C}}\text{CH}_3$) were observed.

3.3. Reaction mechanism

As shown in Scheme 1, the UV irradiation of the matrix chloroacetone/Ar leads to; (1) rotational isomerisation from *gauche*- to *syn*-chloroacetone, (2) tautomerisation to hypochlorous acid 1-methylethenyl ester and (3) C–Cl bond fission to form a cyclopropanone $\cdots\text{HCl}$ complex and $\text{CH}_2=\text{C}=\text{O}$. The CH_2COCH_3 formed by the C–Cl bond fission in chloroacetone underwent subsequent H-atom abstraction to form cyclopropanone and dissociation to CH_3 and $\text{CH}_2=\text{C}=\text{O}$. Following the primary product formation, secondary photolyses were observed, leading to the formation of $\text{CH}_2=\text{CH}_2$, CO and 2-chloro-2-methyloxirane. During the reaction of $\text{CH}_2\text{ClCOCH}_3$ in the vapor phase, CH_2COCH_3 was detected [8]. However, in the present study no bands indicative of the formation of CH_2COCH_3 were observed, judging from the comparison with the calculated spectrum. This is probably due to the cage effect that makes subsequent addition and abstraction reactions effective.

Unlike the photoinduced reactions of chloroacetyl chloride [24] and *o*-fluorobenzoyl chloride [30] in solid Ar, where the rotational isomerisation reached an equilibrium and the less stable conformer was decomposed upon further irradiation, in our case the concentration of *syn*-chloroacetone continued to grow during the entire irradiation period, as shown in Figure 2. This might indicate that in the photolysis of

syn-CH₂=COClCH₃ a considerable amount of chloroacetone is produced by recombination, in parallel to the formation of 2-chloro-2-methyloxirane.

4. Conclusions

UV light-induced reactions of chloroacetone in a cryogenic Ar matrix were investigated using infrared spectroscopy. The photoinduced isomerisations of *gauche*-chloroacetone to *syn*-chloroacetone and hypochlorous acid 1-methylethenyl ester were confirmed by comparison with the calculated spectra. In addition, the photolysis products were found to be CH₂=C=O, a cyclopropanone...HCl complex, HCl and CO. The cyclopropanone...HCl complex was further decomposed into CH₂=CH₂, CO and HCl. The hypochlorous acid 1-methylethenyl ester was further isomerized to 2-chloro-2-methyloxirane.

Figure captions

Figure 1. IR difference spectra upon UV irradiation of the matrix chloroacetone/Ar = 1/500 obtained by the spectral subtraction of (a) 70–0 min and (b) 280–200 min. Calculated infrared spectra of (c) *gauche*- (downward) and *syn*-chloroacetone (upward) and (d) *syn*- (upper) and *gauche*-CH₂=COClCH₃ (lower) at the B3LYP/6-311++G(2d,2p) level with anharmonic correction.

Figure 2. Absorbance changes of the bands at 977 (□), 960 (●), 934 (×) and 838 (Δ) cm⁻¹ upon UV irradiation of the chloroacetone/Ar = 1/500 (a) without and (b) with a UV-29 filter.

Figure 3. Optimized structures of (a) *syn*- and (b) *gauche*-CH₂=COClCH₃ at the B3LYP/aug-cc-pV(T+d)Z level.

Figure S1. Normalized absorbance changes of the bands at 2745 (□), 2139 (×) and 960 (●) cm⁻¹ upon UV irradiation of the chloroacetone/Ar = 1/500 without a UV-29 filter.

References

- [1] M.J. Molina, F.S. Rowland, *Nature* 249 (1974) 810.
- [2] M. Kanakidou, J.H. Seinfeld, S.N. Pandis, I. Barnes, F.J. Dentener, M.C. Facchini, R. Van Dingenen, B. Ervens, A. Nenes, C.J. Nielsen, E. Swietlicki, J.P. Putaud, Y. Balkanski, S. Fuzzi, J. Horth, G.K. Moortgat, R. Winterhalter, C.E.L. Myhre, K. Tsigaridis, E. Vignati, E.G. Stephanou, J. Wilson, *Atmos. Chem. Phys.* 5 (2005) 1053.
- [3] G. Myhre, D. Shindell, F.-M. Bréon, W. Collins, J. Fuglestad, J. Huang, D. Koch, J.-F. Lamarque, D. Lee, B. Mendoza, T. Nakajima, A. Robock, G. Stephens, T. Takemura and H. Zhang, 2013: Anthropogenic and Natural Radiative Forcing. In:

Climate Change 2013: The Physical Science Basis. Contribution of Working Group I to the Fifth assessment Report of the Intergovernmental Panel on Climate Change [T. F. Stocker, D. Qin, G.-K. Plattner, M. Tignor, S.K. Allen, J. Boschung, A. Nauels, Y. Xia, V. Bex and P.M. Midgley (eds.)]. Cambridge, United Kingdom and New York, NY, USA.

[4] S. Carr, D.E. Shallcross, C. Canosa-Mas, J.C. Wenger, H.W. Sidebottom, J.J. Treacy, R.P. Wayne, *Phys. Chem. Chem. Phys.* 5 (2003) 3874.

[5] N. Tanaka, S. Yamagishi, H. Nishikiori, *Comput. Theor. Chem.* 1020 (2013) 108.

[6] G.C.G. Waschewsky, P.W. Kash, T.L. Myers, D.C. Kitchen, L.J. Butler, *J. Chem. Soc. Faraday Trans.* 90 (1994) 1581.

[7] D.C. Kitchen, T.L. Myers, L.J. Butler, *J. Phys. Chem.* 100 (1996) 5200.

[8] B.W. Alligood, B.L. FitzPatrick, D.E. Szpunar, L.J. Butler, *J. Chem. Phys.* 134 (2011) 054301.

[9] S. Mizushima, T. Shimanouchi, T. Miyazawa, I. Ichishima, K. Kuratani, I. Nakagawa, N. Shido, *J. Chem. Phys.* 21 (1953) 815.

[10] S.A. Guerrero, J.R.T. Barros, B. Wladidlaw, R. Rittner, P.R. Olivato, *J. Chem. Soc. Perkin Trans. II* (1983) 1053.

[11] J.R. Durig, L. Jie, C.L. Tolley, T.S. Little, *Spectrochim. Acta A* 47 (1991) 105.

[12] Q. Shen, K. Hagen, *J. Phys. Chem.* 95 (1991) 7655.

[13] T.R. Doi, F. Yoshinaga, C.F. Tormena, R. Rittner, R.J. Abraham, *Spectrochim. Acta A* 61 (2005) 2221.

[14] M.J. Frisch, G.W. Trucks, H.B. Schlegel, G.E. Scuseria, M.A. Robb, J.R. Cheeseman, G. Scalmani, V. Barone, B. Mennucci, G.A. Petersson, H. Nakatsuji, M. Caricato, X. Li, H.P. Hratchian, A.F. Izmaylov, J. Bloino, G. Zheng, J.L. Sonnenberg, M. Hada, M. Ehara, K. Toyota, R. Fukuda, J. Hasegawa, M. Ishida, T. Nakajima, Y. Honda, O. Kitao, H. Nakai, T. Vreven, J. J. A. Montgomery, J.E. Peralta, F. Ogliaro, M. Bearpark, J.J. Heyd, E. Brothers, K.N. Kudin, V.N. Staroverov, T. Keith, R. Kobayashi, J. Normand, K. Raghavachari, A. Rendell, J.C. Burant, S.S. Iyengar, J. Tomasi, M. Cossi, N. Rega, J.M. Millam, M. Klene, J.E. Knox, J.B. Cross, V. Bakken, C. Adamo, J. Jaramillo, R. Gomperts, R.E. Stratmann, O. Yazyev, A.J. Austin, R. Cammi, C. Pomelli, J.W. Ochterski, R.L. Martin, K. Morokuma, V.G. Zakrzewski, G.A. Voth, P. Salvador, J.J. Dannenberg, S. Dapprich, A.D. Daniels, O. Farkas, J.B. Foresman, J.V. Ortiz, J. Cioslowski, D.J. Fox, Gaussian 09, Revision D.01, Wallingford CT, Gaussian, Inc.

[15] C. Lee, W. Yang, R.G. Parr, *Phys. Rev. B* 37 (1988) 785.

[16] A.D. Becke, *J. Chem. Phys.* 98 (1993) 5648.

[17] M.H. Jamróz, *Vibrational Energy Distribution Analysis: VEDA 4*, program,

Warsaw, 2004-2010.

- [18] M. Nakata, H. Frei, *J. Am. Chem. Soc.* 114 (1992) 1363.
- [19] S.B.H. Bach, B.S. Ault, *J. Phys. Chem.* 88 (1984) 3600.
- [20] L. Ballard, G. Henderson, *J. Phys. Chem.* 95 (1991) 660.
- [21] N. Tanaka, Y. Urashima, H. Nishikiori, T. Fujii, *Int. Electron. J. Mole. Design* 2 (2003) 723.
- [22] N. Tanaka, *Open J. Phys. Chem.* 4 (2014) 117.
- [23] T. Tamezane, N. Tanaka, H. Nishikiori, T. Fujii, *Chem. Phys. Lett.* 423 (2006) 434.
- [24] N. Tanaka, M. Nakata, *Int. Res. J. Pure Appl. Chem.* 4 (2014) 762.
- [25] T.F. Thomas, H.J. Rodriguez, *J. Am. Chem. Soc.* 93 (1971) 5918.
- [26] S. Yamabe, T. Minato, Y. Osamura, *J. Am. Chem. Soc.* 101 (1979) 4525.
- [27] G.L. Cui, Y.J. Ai, W.F. Fang, *J. Phys. Chem. A* 114 (2010) 730.
- [28] G.L. Cui, W.H. Fang, *J. Phys. Chem. A* 115 (2011) 1547.
- [29] E. Rytter, D. Gruen, *Spectrochim. Acta* 35A (1979) 199.
- [30] N. Tanaka, K. Nakamura, M. Yutaka, H. Nishikiori, *Chem. Phys. Lett.* 613 (2014) 34.

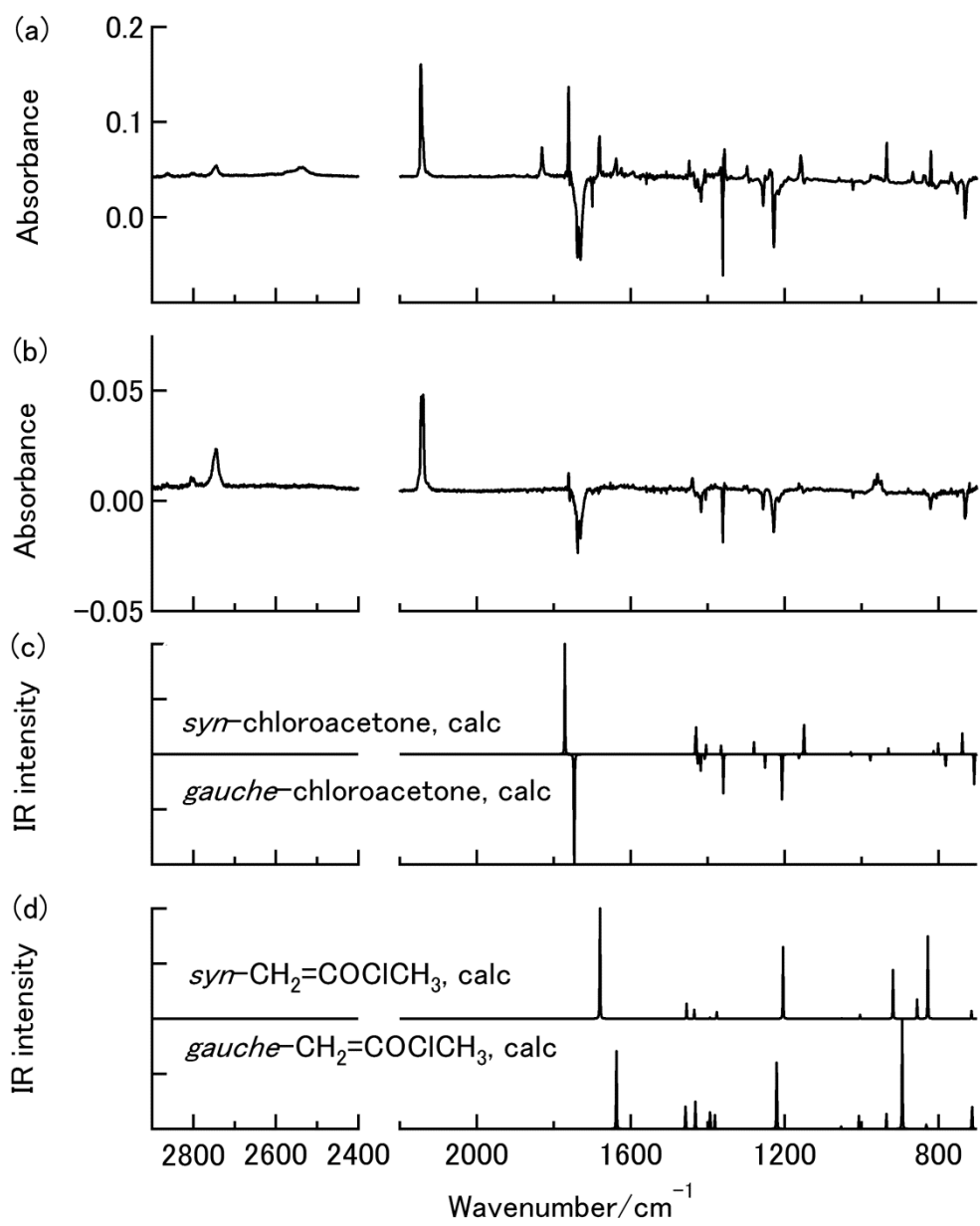


Fig. 1

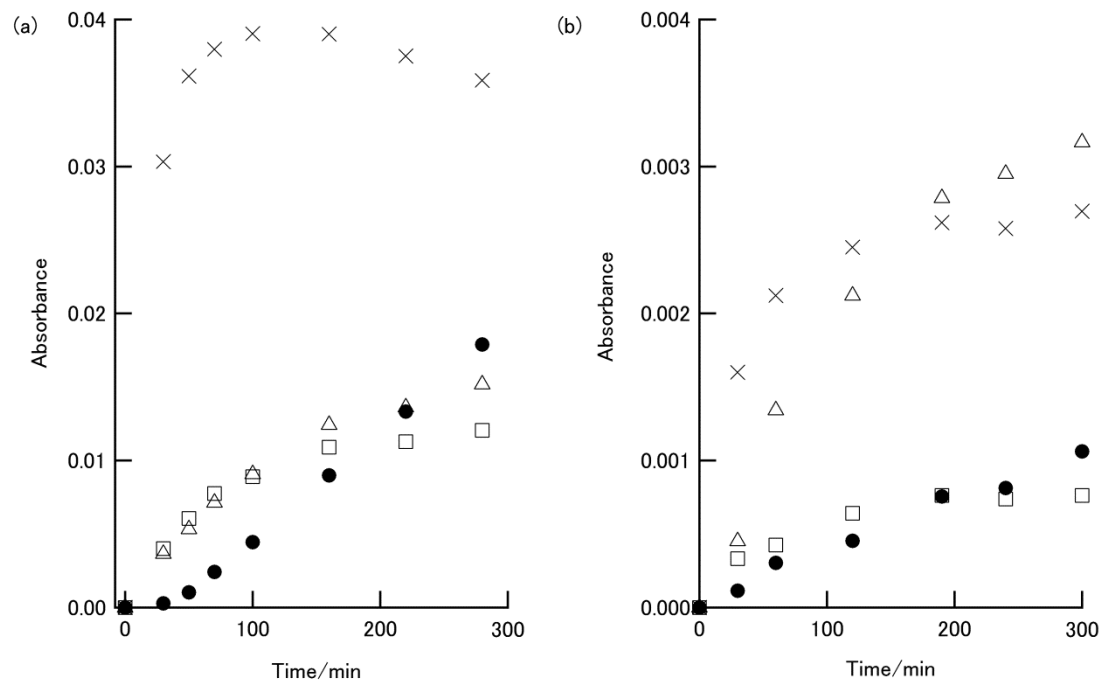
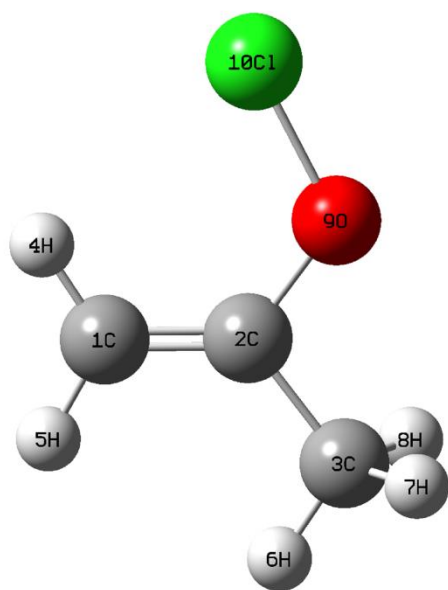


Fig. 2

(a)



(b)

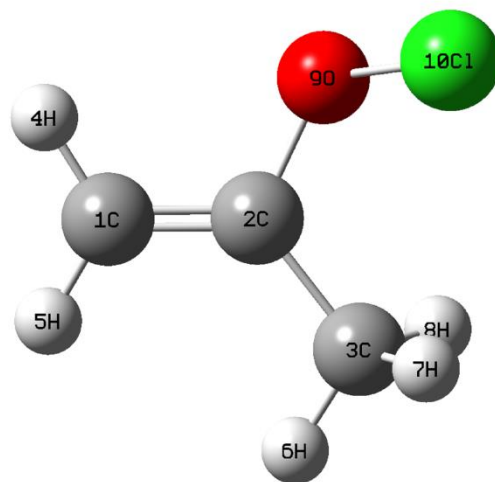


Fig. 3

Table 1

Observed and calculated wavenumbers of photoproducts obtained upon UV irradiation of a matrix chloroacetone/Ar.

Wavenumber/cm ⁻¹		species
obs	calc ^a	
2934	2950	<i>syn</i> -CH ₂ =COClCH ₃
2863		
2805		HCl
2745	2698	HCl⋯CH ₂ =CH ₂
2542	2490	HCl⋯cyclopropanone
2146	2166	CH ₂ =C=O
2139	2186	CO
1831	1827	cyclopropanone⋯HCl
1761	1771	<i>syn</i> -CH ₂ ClCOCH ₃
1681	1680	<i>syn</i> -CH ₂ =COClCH ₃
1448	1455	<i>syn</i> -CH ₂ =COClCH ₃
1440	1451	CH ₂ =CH ₂ ⋯HCl
1436	1435	<i>syn</i> -CH ₂ =COClCH ₃
1407	1376	<i>syn</i> -CH ₂ =COClCH ₃
1381	1390	2-chloro-2-methyloxirane
1306	1347	2-chloro-2-methyloxirane
1298	1280	<i>syn</i> -CH ₂ ClCOCH ₃
1237	1204	<i>syn</i> -CH ₂ =COClCH ₃
1163	1138	2-chloro-2-methyloxirane
1158	1150	<i>syn</i> -CH ₂ ClCOCH ₃
1058	1052	cyclopropanone⋯HCl
976	944	cyclopropanone⋯HCl
966/960/954/949	987	CH ₂ =CH ₂ ⋯HCl
935	919	<i>syn</i> -CH ₂ =COClCH ₃
879	870	2-chloro-2-methyloxirane
867	856	<i>syn</i> -CH ₂ =COClCH ₃
838	801	<i>syn</i> -CH ₂ ClCOCH ₃
820	828	<i>syn</i> -CH ₂ =COClCH ₃
767	739	<i>syn</i> -CH ₂ ClCOCH ₃

^aAnharmonic wavenumbers calculated at the B3LYP/6-311++G(2d,2p) level.

Table 2

Observed and calculated wavenumbers of *syn*-hypochlorous acid 1-methylethenyl ester.

obs		calc ^a			PED \geq 10%	assignment ^b
v/cm ⁻¹	relative intensity	harmonic v/cm ⁻¹	anharmonic v/cm ⁻¹	intensity/km mol ⁻¹		
		3270.6	3129.1	3.0	99vCH	v _a CH ₂
		3183.8	3033.1	0.2	99vCH	v _s CH ₂
		3136.1	3001.3	5.2	92vCH	v _a CH ₃
		3098.7	2957.4	9.8	99vCH	v _a CH ₃
2934	13	3046.7	2950.3	14.2	92vCH	v _s CH ₃
1681	100	1714.2	1680.3	99.8	81vCC	vC=C
1448	32	1495.4	1455.0	10.2	68δCH 18τHCCC	+ δ _a CH ₃
1436	9	1474.2	1434.9	6.4	78δCH 12τHCCC	+ δ _a CH ₃
		1435.6	1393.7	1.1	79δCH	δ _s CH ₃ , δ _s CH ₂ scissor
1407	13	1408.7	1376.3	5.6	93δCH	δ _s CH ₃ , δ _s CH ₂ scissor
1237	29	1239.1	1204.1	49.9	34vCO + 29δCH	vCO
					63τHCCC	+
		1074.9	1051.9	0.2	20δCH	+ γCH ₃ rock
					11γOCCC	
		1017.2	1003.8	2.9	58τHCCC 24δCH	+ δCH ₃ rock
935	96	939.1	918.9	33.6	55vCO + 37δCH	vCO
867	25	873.2	855.8	14.7	80vCC	vCC
820	89	851.0	828.0	55.6	92γCH	γCH ₂ wagging
		723.9	714.9	5.3	58vOCl 27δCCO	+ vOCl
		718.8	711.5	0.0	86τHCCO	τHCCO
		501.5	497.0	3.3	71γOCCC 11τHCCC	+ γOCCC
					45δCCO	
		493.3	494.6	3.8	+16δCCC 15vOCl + 10δCH	+ δCCO

365.6	368.7	0.8	65 δ CCC 17 ν OCl	+	δ CCC
261.6	262.8	0.5	87 δ COCl		δ COCl
168.2	172.1	0.0	85 τ HCCC		τ HCCC
103.6	111.0	3.0	97 τ CCOC		τ CCOC

^aCalculated at the B3LYP/6-311++G(2d,2p) level.

^b ν : stretching; δ : in-plane bending; γ : out-of-plane bending; τ : torsion.

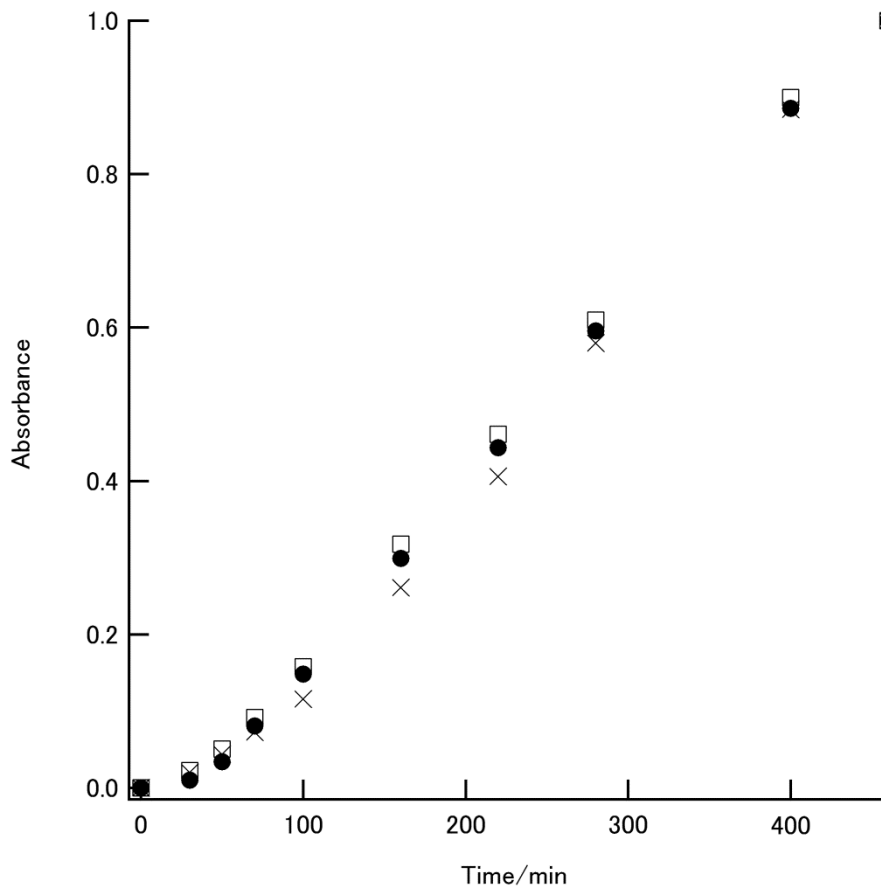


Fig. S1

Table S1

Optimized geometrical parameters of *syn*-hypochlorous acid 1-methylethenyl ester at the B3LYP/aug-cc-pV(T+d)Z and MP2/sug-cc-pV(T+d)Z levels.

Parameters	B3LYP/aug-cc-pV(T+d)Z	MP2/aug-cc-pV(T+d)Z
Bond length/Å		
C1–C2	1.326	1.333
C2–C3	1.498	1.493
C1–H4	1.078	1.077
C1–H5	1.078	1.078
C3–H6	1.087	1.087
C3–H7	1.091	1.089
C3–H8	1.091	1.089
C2–O9	1.386	1.385
O9–Cl10	1.700	1.688
Bond angle/°		
C3–C2–C1	126.6	126.7
H4–C1–C2	122.6	122.6
H5–C1–C2	119.1	118.1
H6–C3–C2	109.7	109.7
H7–C3–C2	110.7	110.3
H8–C3–C2	110.7	110.3
O9–C2–C3	106.9	106.9
Cl10–O9–C2	116.9	115.2
Dihedral angle/°		
H4–C1–C2–C3	180.0	180.0
H5–C1–C2–C3	0.0	0.0
H6–C3–C2–C1	0.0	0.0
H7–C3–C2–C1	–120.3	–120.3
H8–C3–C2–C1	120.3	120.3
O9–C2–C3–C1	180.0	180.0
Cl10–O9–C2–C3	180.0	180.0